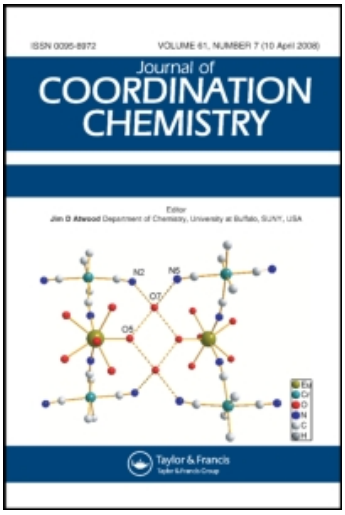

Journal of Coordination Chemistry
Publication details, including instructions for authors and subscription information:
http://www.informaworld.com/smpp/title~content=t713455674

Crystal structure and the magnetic properties of *tris*(2-chloromethyl-4-oxo-4*H*-pyran-5-olato-κ²O⁵,O⁴)iron(III)

K. Hryniewicz[a]; K. Stadnicka[a]; A. Adamski[a]; A. Pattek-Janczyk[a]
[a] Faculty of Chemistry, Jagiellonian University, Kraków, Poland

Online publication date: 07 April 2010

To cite this Article Hryniewicz, K. , Stadnicka, K. , Adamski, A. and Pattek-Janczyk, A.(2010) 'Crystal structure and the magnetic properties of *tris*(2-chloromethyl-4-oxo-4*H*-pyran-5-olato-κ²O⁵,O⁴)iron(III)', Journal of Coordination Chemistry, 63: 6, 977 — 987
To link to this Article: DOI: 10.1080/00958971003686692
URL: http://dx.doi.org/10.1080/00958971003686692

Journal of Coordination Chemistry
Vol. 63, No. 6, 20 March 2010, 977–987

Taylor & Francis
Taylor & Francis Group

Crystal structure and the magnetic properties of *tris*(2-chloromethyl-4-oxo-4*H*-pyran-5-olato-κ^2O^5,O^4)iron(III)

K. HRYNIEWICZ, K. STADNICKA, A. ADAMSKI and A. PATTEK-JANCZYK*

Faculty of Chemistry, Jagiellonian University, Kraków, Poland

(*Received 16 November 2009; in final form 17 November 2009*)

The *tris*(2-chloromethyl-4-oxo-4*H*-pyran-5-olato-κ^2O^5,O^4)iron(III), [Fe(kaCl)$_3$], has been synthesized and characterized by the crystal structure analysis, magnetic susceptibility measurements, Mössbauer, and EPR spectroscopic methods. The X-ray single crystal analysis of [Fe(kaCl)$_3$] revealed a *mer* isomer. The magnetic susceptibility measurements indicated the paramagnetic character in the temperature range of 2 K–298 K. The EPR and Mössbauer spectroscopy confirmed the presence of an iron center in a high-spin state. Additionally, the temperature-independent Mössbauer magnetic hyperfine interactions were observed down to 77 K. These interactions may result from spin–spin relaxation due to the interionic Fe^{3+} distances of 7.386 Å.

Keywords: Iron(III) hydroxypyrone complexes; *mer* Isomers; Crystal structure; Magnetic susceptibility; Mössbauer spectroscopy

1. Introduction

A hydroxypyrone, 2-chloromethyl-5-hydroxy-4*H*-pyran-4-one, known as chlorokojic acid (HkaCl), has biological activity, antimicrobial, and antifungal properties [1, 2]. It forms a monoanionic bidentate ligand through the enolate and carbonyl oxygens, such as kojic acid, maltol or ethyl maltol, hydroxypyrones occurring in nature. Thus, it is expected that HkaCl will show the similar chelating properties toward iron(III), aluminium(III), or vanadium(IV), as the natural hydroxypyrones, complexes of which were tested as new agents for diabetes and anemia therapies [3–6].

The complexes of ligands with similar functional groups have been reviewed by Nadia El-Gamel [7]; the interactions of metal ions with oxicams, the anti-inflammatory drugs. Depending on the metal bound, the oxicams were monoanionic monodentate [with Pt(II)], bidentate [with Cu(II) and Cd(II)], or tridentate [with organotin] agents. In complexes with Fe(III) isoxicam, piroxicam, and tenoxicam coordinate iron through

*Corresponding author. Email: patjan@chemia.uj.edu.pl

ISSN 0095-8972 print/ISSN 1029-0389 online
DOI: 10.1080/00958971003686692

the enolate oxygen and the carbonyl oxygen of the amide group, i.e., bidentate coordination similar to the hydroxypyrone complexes.

The octahedral complexes of hydroxypyrones may crystallize as *fac* or *mer* isomers. The *fac* isomers were found in the case of iron(III) complexes with ethyl maltol and kojic acid [8, 9], while the *mer* isomer was observed for *tris*(maltolato)iron(III) [10]. The reason for either *fac* or *mer* isomer formation has not yet been explained. In our previous studies [11], some efforts to predict the molecular structure of iron complexes with chlorokojic acid and allomaltol were undertaken. The expected structure and properties of $[Fe(kaCl)_3]$ were confirmed by present studies.

2. Experimental

2.1. *HkaCl*

HkaCl was prepared according to the procedure given in literature [12]. Kojic acid (Sigma Aldrich) was dissolved in freshly distilled thionyl chloride. After stirring for 1 h, an yellowish crystalline product was formed. The precipitate was filtered, washed with petroleum ether, and recrystallized (twice) from aqueous solution. Pure chlorokojic acid as colorless needles was obtained. Anal. Calcd for $C_6ClH_5O_3$ (%): C, 44.9; H, 3.1. Found: C, 44.8; H, 3.3.

2.2. *[Fe(kaCl)$_3$]*

Iron perchlorate (Sigma Aldrich) and chlorokojic acid in molar ratio 1 : 8 were dissolved in water–ethanol (1 : 1) solution. Dark red crystals of $[Fe(kaCl)_3]$ were obtained from the purple solution after slow crystallization (taking about 2 months) at ambient temperature. Anal. Calcd for $FeC_{18}Cl_3H_{15}O_9$ (%): C, 40.4; H, 2.3; Fe, 10.4. Found: C, 40.4; H, 2.4; Fe, 10.1.

2.3. *X-ray crystal structure analysis*

X-ray diffraction measurements were performed with a Nonius Kappa-CCD diffractometer using graphite monochromated Mo-Kα radiation at room temperature. The details of data collection and cell refinement are shown in table 1. Lorentz, polarization, and absorption corrections were introduced using DENZO and HKL Scalepack [13]. The structure was found by direct methods using SIR-92 [14] and refined by full-matrix least squares based on F^2 using SHELXL-97 [15]. The positions of hydrogen atoms, calculated from the geometrical constraints with methylene C–H = 0.97 Å, aromatic C–H = 0.93 Å, were introduced into refinement in the riding model with displacement parameters $U_{iso} = 1.2U_{eq}$ of the parent atom.

Table 1. Crystallographic data and processing parameters for [Fe(kaCl)$_3$].

Empirical formula	$C_{18}H_{12}Cl_3FeO_9$
Formula weight	534.48
Temperature (K)	293(2)
Wavelength (Å)	0.71073
Crystal system	Monoclinic
Space group	*P2(1)/c*
Unit cell dimensions (Å, °)	
a	15.3917(3)
b	11.4184(3)
c	11.7016(5)
β	100.449(2)
Volume (Å^3), *Z*	2022.4(1), 4
Calculated density (Mgm^{-3})	1.755
Absorption coefficient (mm^{-1})	1.193
F(000)	1076
Crystal size (mm^3)	$0.17 \times 0.12 \times 0.12$
Crystal form, color	Prism, dark red
θ range for data collection (°)	2.23–27.50
Diffractometer	Nonius Kappa-CCD
Data collection method	ϕ scans ($\kappa = 0$) + ω scans
Limiting indices	$0 \le h \le 19$; $-14 \le k \le 14$; $-15 \le l \le 14$
Reflections collected	8749
Independent reflection	4619 [R(int) = 0.0289]
Reflections observed [$I > 2\sigma(I)$]	3382
Completeness to $\theta = 25.02$ (%)	99.6
Absorption correction [13]	Multi-scan
Max. and min. transmission	0.8229 and 0.8701
Data/restraints/parameters	4619/0/280
Goodness-of-fit parameter (S)	1.101
Final R indices [$I > 2\sigma(I)$]	$R_1 = 0.0569$, $wR_2 = 0.1159$
R indices (all data)	$R_1 = 0.0827$, $wR_2 = 0.1251$
Weighting scheme w: A, B	0.0240, 4.1897
Largest difference peak and hole (e Å^{-3})	0.667 and −0.492

$w = 1/[\sigma^2(F_o^2) + (AP)^2 + BP]$, where $P = (F_o^2 + 2F_c^2)/3$.

2.4. *Physical methods*

The magnetic susceptibility measurements of the powdered sample were performed in a Quantum Design SQUID magnetometer MPMS−XL5. The magnetization was measured at the constant temperature of 2 K in the variable magnetic field of 0–5 T (to 4000×10^3 A m^{-1}) and at the constant magnetic field of 5 T (4000×10^3 A m^{-1}) in the temperature range of 2–293 K.

The CW-EPR X-band spectra were measured at ambient and liquid nitrogen temperatures with a Bruker ELEXSYS E500 spectrometer operating at 100 kHz field modulation. The EPR parameters were evaluated by using an SIM32 simulation program [16].

The Mössbauer spectra were measured at two temperatures, 298 and 80 K, using a conventional spectrometer in transmission geometry with a ^{57}Co/Rh source. The absorbent was prepared as a pellet with a thickness of *ca* 10 mg Fe cm^{-2}. The spectra were analyzed numerically by means of the Voigt-based fitting method of Rancourt and Ping for hyperfine field distributions (HFD) [17]. The isomer shift values were quoted relative to α–Fe and the full width at half maximum was fixed at 0.24 mm s^{-1}.

3. Results and discussion

3.1. *Structural data*

$Fe(kaCl)_3$ crystallizes in the monoclinic system, space group *P2(1)/c* with the unit cell containing four molecules of the complex. The molecule with atom labeling scheme is shown in figure 1. Three symmetry-independent anionic ligands coordinate to iron through oxygens from the dissociated hydroxyl C–O^- [O(8a), O(8b), O(8c)] and carbonyl C=O [O(7a), O(7b), O(7c)] groups. The octahedron distorts toward trigonal antiprism. Ligand "b" is oriented differently from the other two, "a" and "c." The complex is *mer* and the angle between the planes of O^- and carbonyl oxygen is close to 90° [86.7(1)°]. The selected geometrical parameters for $[Fe(kaCl)_3]$ are given in tables 2 and 3.

In ligand "b", C–O^- (1.301 Å) and C=O (1.281 Å) bond length values are relatively close to each other in comparison to those determined for "a" and "c." In "a", C–O^- = 1.322 Å and C=O = 1.276 Å, and in "c", C–O^- = 1.323 Å and C=O = 1.270 Å, reveal greater difference. The C(2b)–C(3b) as well as C(5b)–C(6b) are significantly elongated when compared to the bonds in the other two ligands, indicating more uniform electron density distribution in "b."

The packing of the complex molecules in the unit cell is shown in figure 2. The structure consists of layers which are 5.239 Å apart and parallel to (10–1). The arrangement of the complex molecules in the layer is shown in figure 3. In the layer, the molecules interact through specific weak interactions, C–Cl···Cg (one for each of the a, b, and c ligands) and C9a–H9a2···Cgb. The geometrical parameters for

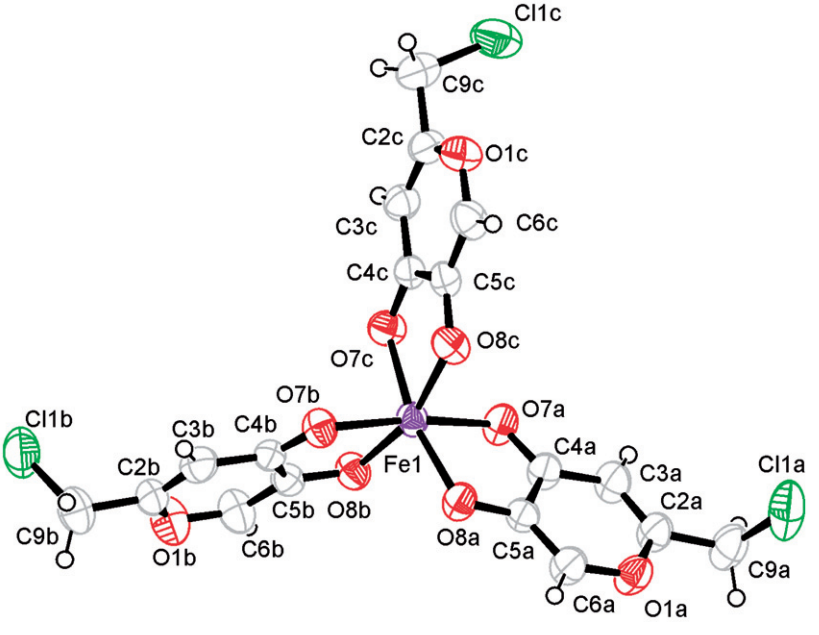

Figure 1. Configuration of $[Fe(kaCl)_3]$ with the atom numbering scheme. Displacement ellipsoids are drawn at 50% probability level. ORTEP03 [26].

Table 2. Selected bond lengths (Å).

	a	b	c
Fe(1)–O(8)	1.974(3)	2.002(3)	1.984(3)
Fe(1)–O(7)	2.057(3)	2.054(3)	2.065(3)
Cl(1)–C(9)	1.795(5)	1.802(5)	1.771(5)
O(7)–C(4)	1.276(4)	1.281(4)	1.270(4)
O(8)–C(5)	1.322(4)	1.301(4)	1.323(4)
O(1)–C(2)	1.342(5)	1.334(5)	1.339(5)
C(3)–C(2)	1.341(6)	1.364(6)	1.337(6)
C(4)–C(3)	1.413(5)	1.409(5)	1.406(5)
C(5)–C(4)	1.438(5)	1.444(5)	1.447(5)
C(5)–C(6)	1.351(5)	1.363(6)	1.353(5)
O(1)–C(6)	1.356(5)	1.343(5)	1.354(5)
C(2)–C(9)	1.484(6)	1.483(6)	1.499(6)

Table 3. Selected valence and torsion angles (°).

O(8a)–Fe(1)–O(7a)	80.4(1)	O(8b)–Fe(1)–O(7b)	80.3(1)	O(8c)–Fe(1)–O(7c)	80.4(1)
O(8c)–Fe(1)–O(7a)	95.8(1)	O(8a)–Fe(1)–O(7b)	96.0(1)	O(8a)–Fe(1)–O(8b)	97.9(1)
O(8b)–Fe(1)–O(7a)	92.0(1)	O(8c)–Fe(1)–O(7b)	92.8(1)	O(8a)–Fe(1)–O(8c)	97.5(1)
O(7a)–Fe(1)–O(7c)	85.6(1)	O(7b)–Fe(1)–O(7c)	98.4(1)	O(8b)–Fe(1)–O(7c)	85.9(1)
O(7b)–Fe(1)–O(7a)	171.0(1)	O(8c)–Fe(1)–O(8b)	163.7(1)	O(8a)–Fe(1)–O(7c)	165.6(1)
O(1a)–C(2a)–C(9a)–Cl(1a)	−75.9(4)	O(1b)–C(2b)–C(9b)–Cl(1b)	−71.0(5)	O(1c)–C(2c)–C(9c)–Cl(1c)	81.8(5)

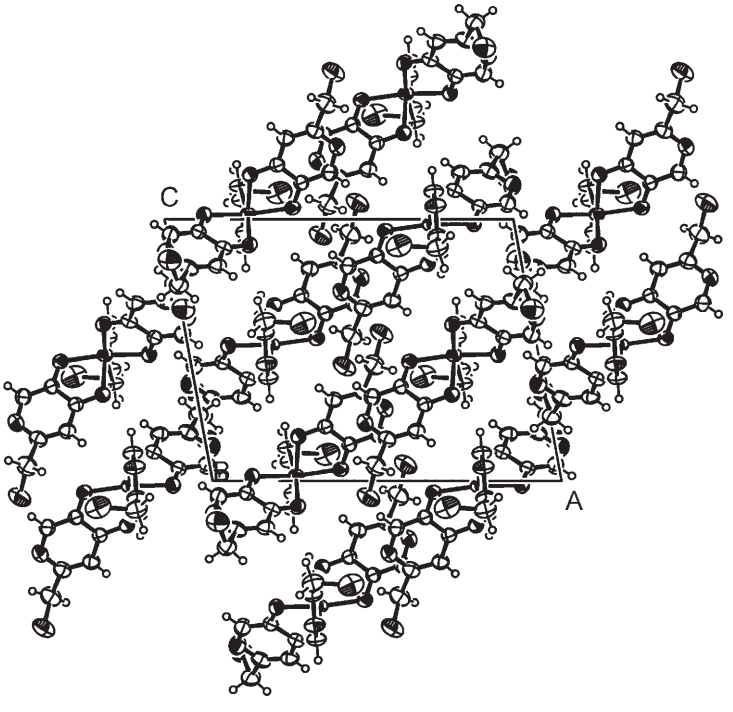

Figure 2. Packing of [Fe(kaCl)$_3$] in the unit cell projected in [0 1 0] direction.

intermolecular interactions are given in table 4. Between the layers, there are only weak C–H···O interactions [18] and C–Cl···Cl halogen interactions [19].

3.2. *Magnetic and spectroscopic properties*

The results of magnetic measurements are shown in figure 4, magnetization *versus* the applied magnetic field, and in figure 5, the variables χ and χ_T *versus* temperature.

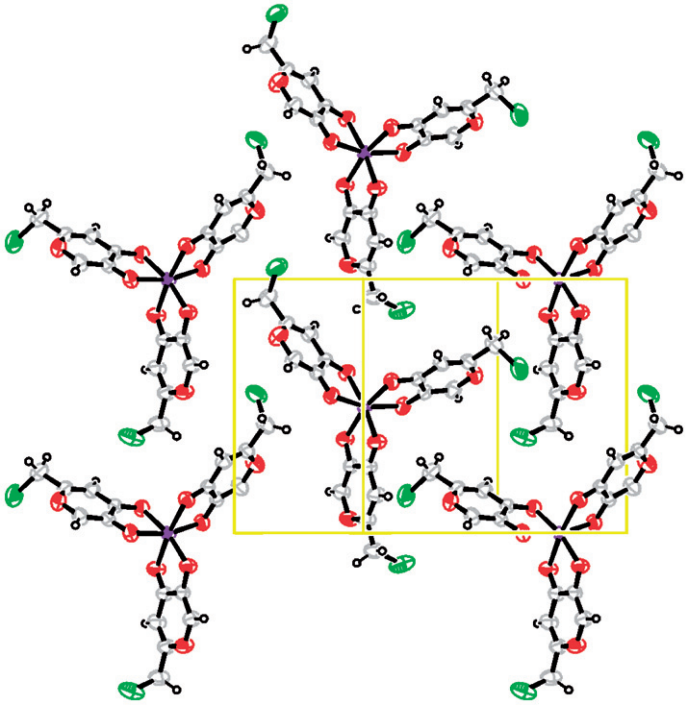

Figure 3. The mutual arrangement of $[Fe(kaCl)_3]$ molecules in the layer.

Table 4. The geometrical parameters of weak interactions (Å, °).

D–H···A	Acceptor position	D–H/Cl	H/Cl···A	D···A	∠DH/ClA	Comment
C3a–H3a···O8a	$x, -y+1/2, z+1/2$	0.93	2.34	3.257	171	Interlayer
C6a–H6a···O7a	$x, -y+1/2, z-1/2$	0.93	2.27	3.173	162	Interlayer
C9a–H9a1···O7b	$x, -y+1/2, z+1/2$	0.97	2.56	3.498	162	Interlayer
C3b–H3b···O7c	$x, -y-1/2, z-1/2$	0.93	2.42	3.353	176	Interlayer
C6b–H6b···O8b	$-x, -y, -z$	0.93	2.52	3.273	138	Interlayer
C9b–H9b1···O8b	$-x, -y-1/2, -z-1/2$	0.97	2.53	3.454	160	Interlayer
C9a–Cl1a···Cl1c	$x, -y+1/2, z-1/2$	1.795	3.504	5.253	163.9	Interlayer
C9c–Cl1c···Cl1a	$x, -y+1/2, z+1/2$	1.771	3.504	3.871	88.0	Interlayer
C9a–H9a2···Cgb	$x, y+1, z$	0.97	3.08	4.037	170	Intralayer
C9a–Cl1a···Cgc	$x, y+1, z$	1.795	3.62	4.890	125.6	Interlayer
C9c–Cl1c···Cga	$x, y+1, z$	1.771	3.58	3.941	88.2	Interlayer
C9b–Cl1b···Cgb	$-x, y-1/2, -z-1/2$	1.802	3.36	3.856	91.5	Interlayer

Cg denotes the gravity center of the pyran ring; Cga, "a" ligand; Cgb, "b" ligand; and Cgc, "c" ligand.

The magnetic measurements carried out at 2 K and variable magnetic field (figure 4) reveal a lack of magnetization hysteresis suggesting paramagnetic character. The magnetic moment $\mu_0 = 4.91(2)\mu_B$, calculated by extrapolation to an infinite magnetic field, is slightly lower than the theoretical one for $g = 2.0$ and

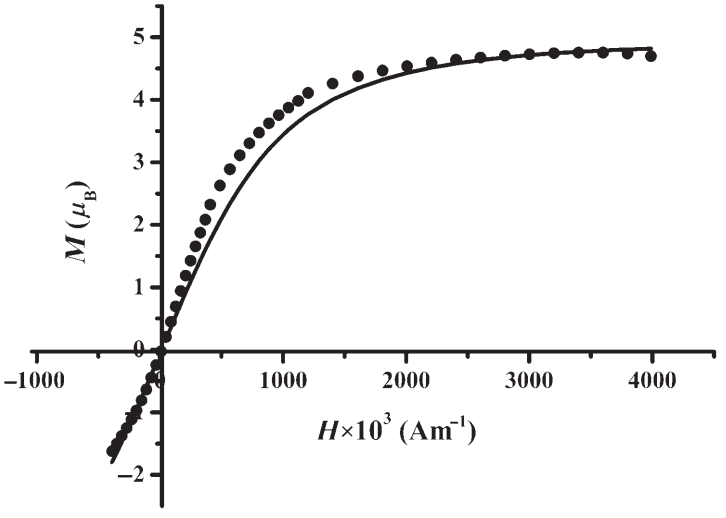

Figure 4. Magnetization *vs.* applied magnetic field for [Fe(kaCl)$_3$].

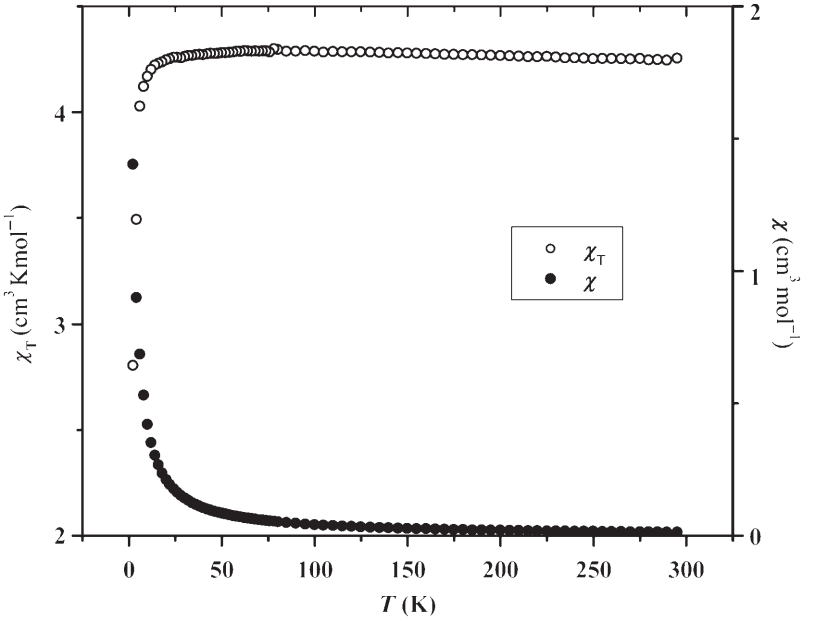

Figure 5. χ and χ_T *vs.* temperature for [Fe(kaCl)$_3$].

$S = 5/2$ ($\mu_0 = 5.00\mu_B$). In the range of 295 K–20 K, the temperature dependence of magnetic susceptibility for [Fe(kaCl)$_3$] (figure 5) revealed a slight deviation from the straight line, indicating the value of χ_T equal to 4.256 cm^3 K mol^{-1} at ambient temperature, reaching a maximum value of 4.301 cm^3 K mol^{-1} at 78 K, and decreasing to 4.247 cm^3 K mol^{-1} at 20 K.

Below 20 K, χ_T decreases significantly to 2.805 cm^3 K mol^{-1} at 2 K. The data can be fit to the Curie–Weiss law with constants $C = 4.256(2)$ cm^3 K mol^{-1} and $\theta = 0.28(2)$ K. The calculated C constant differs slightly (2.7%) from the value expected for high-spin iron(III) ion, perhaps by very weak ferromagnetic interactions occurring in the studied complex.

The EPR spectra recorded at ambient and liquid nitrogen temperatures (figure 6) revealed similar shapes. The spectral lines are distinctly broadened ($\Delta B_{pp} \approx 1000$ G) with a broad maximum at $g \approx 4.0$, which is a little bit lower than $g \approx 4.3$ usually ascribed to $|3/2\rangle$ Kramer's doublet for strongly distorted iron d orbitals of iron(III) in a high-spin state [20–22]. The low-temperature spectrum also shows a weak broad maximum ($\Delta B_{pp} \approx 1000$ G) at $g \approx 1.7$–2.0, which may be attributed to the ground Kramer's doublet: $|1/2\rangle$, when $D > 0$, or $|5/2\rangle$, when $D < 0$. For $E/D \approx 1/3$ (D and E are the axial and rhombic zero-field splitting (ZFS) parameters, respectively), g factor of the ground doublet is strongly anisotropic [23], thus its signal is rather difficult to detect. The occupancy of Kramer's doublets changes with temperature, resulting in an additional weak maximum in the low temperature spectrum of [Fe(kaCl)$_3$]. The EPR studies suggest strong deviation from the octahedral geometry of the $^6A_1$ ground state of Fe(III) in a high-spin state.

The line shapes of [Fe(kaCl)$_3$] Mössbauer spectra (figure 7) may be ascribed as non-Lorentzian, asymmetric singlets, very similar to the line shape of Mössbauer spectra of *tris*(kojato)iron(III) [9]. It is very likely that the same interactions are present in both complexes. The asymmetry of the observed singlet suggests the presence of quadrupole interactions, whereas the wide absorption range from -2.5 to $+3$ mm s^{-1} may indicate magnetic hyperfine interactions. The Mössbauer parameters of [Fe(kaCl)$_3$] are characteristic of the high-spin Fe^{3+} ions (table 5).

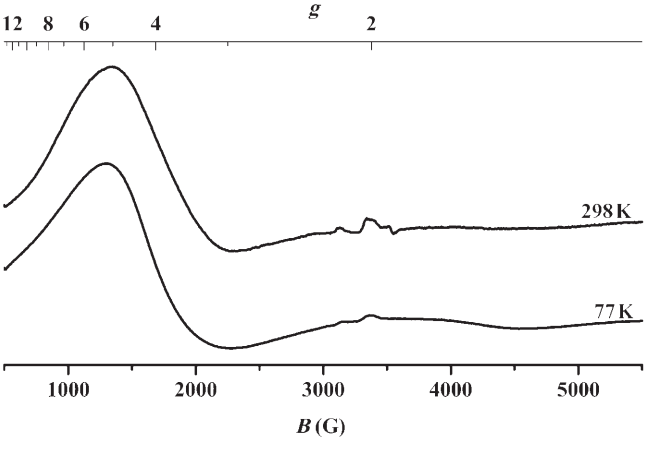

Figure 6. EPR spectra of [Fe(kaCl)$_3$].

The quadrupole interactions arise from distortion of the octahedron in the first coordination sphere and additionally from the different electron distribution at O7 and O8. The obtained values of quadrupole splitting (QS) are similar to those found for [Fe(ka)$_3$] [9]. However, for [Fe(kaCl)$_3$] these parameters decrease with decreasing temperature, whereas in [Fe(ka)$_3$] they behave in an opposite way. The distance between iron ions in [Fe(kaCl)$_3$] (7.38 Å) is comparable to the distance found in other iron complexes with bidentate oxygen donors, *e.g.* Fe···Fe = 7.6 Å for ferric acetylacetonate [24] and Fe···Fe = 6.86 Å for sodium *tris*-malonatoferrate(III) octahydrate [25], for which spin–spin relaxation phenomena were suggested. The temperature dependence of the average hyperfine field H as well as its distribution, which increase with decreasing temperature, may indicate strong d orbitals distortion and Kramer's doublet splitting, in agreement with the EPR spectra.

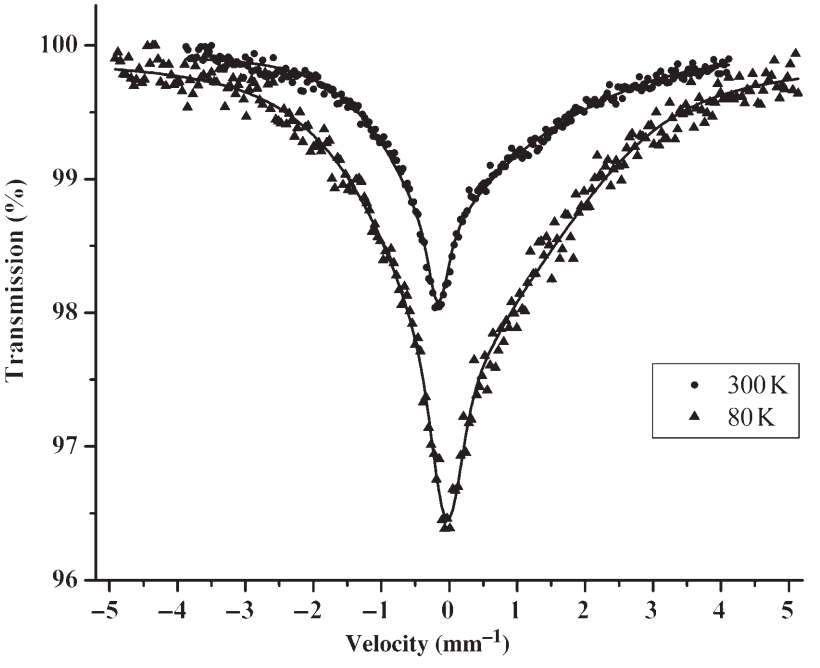

Figure 7. Mössbauer spectra of [Fe(kaCl)$_3$].

Table 5. Mössbauer parameters for [Fe(kaCl)$_3$].

Temperature (K)	IS (mms^{-1})	QS (mms^{-1})	$H_{average}$ (T)	σH (T)
300	0.33	0.52	0.49	9.05
80	0.44	0.47	0.71	13.15

4. Conclusions

The iron(III) complex with chlorokojic acid confirmed the structure of $[Fe(kaCl)_3]$ as a *mer* isomer, expected from the geometrical features of chlorokojic acid, HkaCl. The similar bond lengths in the HkaCl pyran ring suggest more probable formation of iron(III) complex in the *mer* than in *fac* configuration. On the other hand, the kojic acid, with two double bonds distinguished in the pyran ring, forms the *fac* isomer.

Similar Fe(III) complexes with isoxicam, tenoxicam, and piroxicam have been reported to show 1:3 Fe(III):ligand stoichiometry in the solid state [27–29], whereas in methanol, the complex stoichiometry was $Fe(oxicam)_2$ and Fe(oxicam) for tenoxicam and piroxicam, respectively, and in acetone three dimers were found for both ligands, $Fe_2(oxicam)$, $Fe_2(oxicam)_2$, and $Fe_2(oxicam)_3$ [30]. The high-spin state of iron in $[Fe(kaCl)_3]$ was confirmed by the EPR and Mössbauer spectroscopies as well as by the magnetic susceptibility measurements. In the temperature range of 2–298 K, the complex has distinct paramagnetic character. Additionally, the spectroscopic results indicate the strong distortion from ideal octahedral geometry due to the various electron densities of oxygen atoms in the first coordination sphere. The magnetic properties of iron complexes with kojic acid derivatives are not significantly influenced by the differences in complex configurations (*fac* or *mer*).

Supplementary material

CCDC 739775 contains supplementary crystallographic data for this article. The data can be obtained free of charge at www.ccdc.cam.ac.uk or from the Cambridge Crystallographic Data Centre, 12 Union Road, Cambridge CB2 1EZ, UK; Fax: +44 1223 336033; Email: deposit@ccdc.cam.ac.uk.

Acknowledgments

The authors are very grateful to Prof. K. Tomala (M. Smoluchowski, Institute of Physics, Jagiellonian University, Kraków, Poland) for the magnetic measurements. The authors thank the X-ray Laboratory Faculty of Chemistry, Jagiellonian University, for making the Nonius KappaCCD diffractometer available.

References

[1] J. Bransova, J. Brtko, M. Uher, L. Novotny. *Int. J. Biochem. Cell Biol.*, **27**, 701 (1995).
[2] M.D. Aytemir, D. Demir Erol, R.C. Hider, M. Ozalp. *Turk. J. Chem.*, **27**, 757 (2003).
[3] G.R. Willsky, A.B. Goldfine, P.J. Kostyniak, J.H. McNeill, L.Q. Yang, H.R. Khan, D.C. Crans. *J. Inorg. Biochem.*, **85**, 33 (2001).
[4] T. Kiss, E. Kiss, E. Garribba, J.H. Sakurai. *J. Inorg. Biochem.*, **80**, 65 (2000).
[5] V.G. Yuen, P. Caravan, L. Gelmini, N. Glover, J.H. McNeill, I.A. Setyawati, Y. Zhou, C. Orvig. *J. Inorg. Biochem.*, **68**, 109 (1997).

[6] D.M. Reffitt, T.J. Burden, P.T. Seed, J. Wood, R.P.H. Thompson, J. Powell. *Ann. Clin. Biochem.*, **37**, 457 (2000).
[7] N.E.A. El-Gamel. *J. Coord. Chem.*, **62**, 2239 (2009).
[8] M. Odoko, K. Yamamoto, M. Hosen, N. Okabe. *Acta Crystallogr., Sect. C*, **59**, 121 (2003).
[9] K. Zaremba, W. Lasocha, A. Adamski, J. Stanek, A. Pattek-Janczyk. *J. Coord. Chem.*, **60**, 1537 (2007).
[10] M.T. Ahmet, C.S. Frampton, J. Silver. *J. Chem. Soc., Dalton Trans.*, 1159 (1988).
[11] K. Hryniewicz, K. Stadnicka, A. Pattek-Janczyk. *J. Mol. Struct.*, **919**, 255 (2009).
[12] Z.D. Liu, S. Piyamongkol, D.Y. Liu, H.H. Khodr, S.L. Lu, R.C. Hider. *Bioorg. Med. Chem.*, **9**, 563 (2001).
[13] Z. Otwinowski, W. Minor. In *Methods in Enzymology, Macromolecular Crystallography, Part A*, C.W. Carter Jr, R.M. Sweet (Eds), Vol. 276, pp. 307–326, Academic Press, New York (1997).
[14] A. Altomare, G. Cascarano, C. Giacovazzo, A. Guagliardi, M.C. Burla, G. Polidori, M. Camalli. *J. Appl. Crystallogr.*, **27**, 435 (1994).
[15] G.M. Sheldrick. *Acta Crystallogr., Sect. A*, **64**, 112 (2008).
[16] T. Spalek, P. Pietrzyk, Z. Sojka. *J. Chem. Inf. Model.*, **45**, 18 (2005).
[17] D.G. Rancourt. *Mosmod Mössbauer Analysis Software, Module 9.2*. (1996); Recommended article: D.G. Rancourt, J.Y. Ping. *Nucl. Instrum. Meth. Phys. Res.*, **B58**, 85 (1991).
[18] G.R. Desiraju, T. Steiner. *The Weak Hydrogen Bond*, Oxford University Press, Oxford (2001).
[19] G.A. Jeffery. *Crystallogr. Rev.*, **9**, 135 (2003).
[20] H. Wu. *J. Mol. Graphics*, **14**, 328 (1996).
[21] H. Wu. *J. Mol. Graphics*, **14**, 338 (1996).
[22] H.H. Wickman, M.P. Klein, D.A. Shirley. *Phys. Rev.*, **152**, 345 (1966).
[23] H. Hummel, E. Bill, T. Weyhermuller, K. Wieghardt. *Inorg. Chim. Acta*, **291**, 258 (1999).
[24] J.W.G. Wignall. *J. Chem. Phys.*, **44**, 2462 (1966).
[25] S. Calogero, L. Stievano, L. Diamandescu, D. Mihaila-Tarabasanu, G. Valle. *Polyhedron*, **16**, 3953 (1997).
[26] L.J. Farrugia. *J. Appl. Crystallogr.*, **30**, 565 (1997).
[27] D.O. Harrison, R. Thomas, A.E. Underhill, J.K. Fletcher, P.S. Gomm, F. Hallway. *Polyhedron*, **4**, 681 (1985).
[28] A. Bury, A.E. Underhill, D.R. Kemp, N.J. O'Shea, J.P. Smith, P.S. Gomm. *Inorg. Chim. Acta*, **128**, 85 (1987).
[29] D.A. Pipe, J.C. Mac Brayne, P.S. Gomm, A.W. Graham, A.E. Underhill, R.J.P. Gomm. *Gazz. Chim. Ital.*, **14**, 463 (1994).
[30] R. Moya-Hernández, R. Gómez-Balderas, A. Mederos, S. Domínguez, M.T. Ramírez-Silva, A. Rojas-Hernández. *J. Coord. Chem.*, **62**, 40 (2009).